

Investigation of the Two-Phase Countercurrent Flow In Structured Packings Using Capacitance Tomography

T. Loser, G. Petritsch, D. Mewes

Institute for Process Engineering,
University of Hannover, Callinstrasse 36, D-30167 Hannover,
Germany, e-mail: dms@c36.uni-hannover.de

Abstract – *The two-phase countercurrent flow in the structured packings BX and Mellapak® of Polypropylene is investigated using capacitance tomography. With this tomographic measurement technique the phase distribution in the cross section of the packed column can be measured without intrusion into the process. The measurements are taken with high temporal resolution of 54 frames per second. Thus even pulses of the flow can be detected. From the reconstructed images the liquid hold-up and the maldistribution of the phases are calculated as a function of time for different gas and liquid loads.*

Keywords: structured packings, maldistribution, capacitance tomography, flooding

1. INTRODUCTION

Structured packings are increasingly popular for the application in packed columns for distillation and absorption processes. Gas and liquid are conducted countercurrently through the packing where the liquid is flowing downwards and the gas upwards. During the last decade structured packings for very high liquid and gas loads and with low pressure drop have been developed [1,2]. These packings help to reduce the investment and operating cost and thus find wide application in chemical and petrochemical industry. However, a high mass transfer can only be obtained if the distribution of the volume fractions and of the velocities of the gas and liquid are uniform all over the packing. Though the constant distribution of the phases at the top and the bottom of the packing is considered carefully, still maldistribution of the two phases occur. This is suspected to be due to two-phase flow instabilities. Therefore the distribution of the phases has to be investigated.

For the investigation of the phase distribution tomographic measurement techniques can be applied. Tomographic measurement techniques have been used for medical imaging for over 20 years and they are now a standard diagnostic tool for many purposes. The use of tomographic imaging techniques in process engineering is becoming increasingly popular. The main advantage of this measuring techniques is the imaging without intrusion into the process. For different applications several possible physical principles for the measurement can be used.

Using many integral measurements taken from different directions across the considered measuring plane or volume the distribution of the considered physical property can be reconstructed mathematically.

The integral measurements can be obtained in numerous ways [3]. There are for example positron or photon emission, γ - and X-ray transmission and scattering, nuclear magnetic resonance, microwave reflection and diffraction, ultrasonic/acoustic techniques, interferometry and holographic tomography, and electrical and electromagnetic field interaction. Depending on the specific technique used different advantages and disadvantages regarding the accuracy, frequency and resolution of the reconstructed images and thus applications can be identified. Furthermore, for industrial applications, the cost of the system as well as the fault-tolerance are important.

Most applications of process tomography in chemical industry require the imaging of fast changing, so called transient processes. This is the case for most multiphase flows of interest. It requires the tomography system to have the capability of very fast data acquisition and, for control purposes, often on-line image reconstruction [4]. Furthermore, the measurement volume is often not a simple circular pipe but a rather complex geometry, such as process equipment containing impellers or catalysts [5,6]. Additionally, if more than two different phases are present, the imaging tasks are even more difficult.

A tomographic measurement technique that is well suited to both research and industrial applications is capacitance tomography. The sensors required for the imaging are robust and relatively cheap and the actual data generation and acquisition well reported [7-10].

The choice of the tomographic measurement system for the investigation of packings is dependent on the spatial and temporal resolution of the system. In Figure 1 several tomographic measuring systems are depicted schematically as a function of their spatial and temporal resolution. In order to achieve high spatial

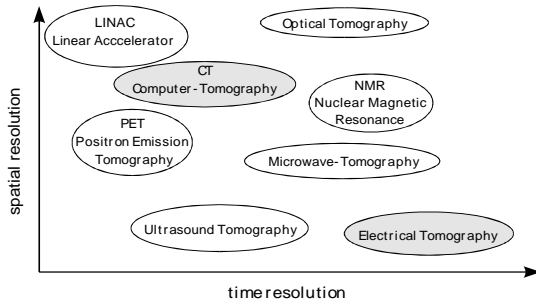


Figure 1: Qualitative comparison of several tomographic measuring systems concerning their spatial and temporal resolution

resolution computer tomography can be applied to measure the distribution of the phases in structured packings. In the past measurements were carried out on dumped packings and structured packings [11-15]. For these measurements, however, the flow in the packing has to be stationary because of the poor temporal resolution. This is only the case for low liquid and gas load when the liquid is trickling down the packing along stationary rivulets or films.

With electrical tomography instead the temporal resolution is high. Time resolutions with more than 50 images per second can be achieved. In structured packings pulsations and flow instabilities are expected close to the flooding point. With the high temporal resolution of capacitance tomography these phenomena can be detected. Therefore in this work capacitance tomography is applied to measure the liquid distribution of the two-phase countercurrent flow in structured packings.

2. CAPACITANCE TOMOGRAPHY

The measurement principle of the capacitance tomography is schematically depicted in Figure 2. Along the circumference of the measurement plane, electrodes are mounted peripherally. The integral measurement values are taken by measuring the capacitance between

two or more electrodes. The measured capacitance is dependent on the permittivity field inside the sensor. If the permittivities of the fluids inside the sensor are different, they can be

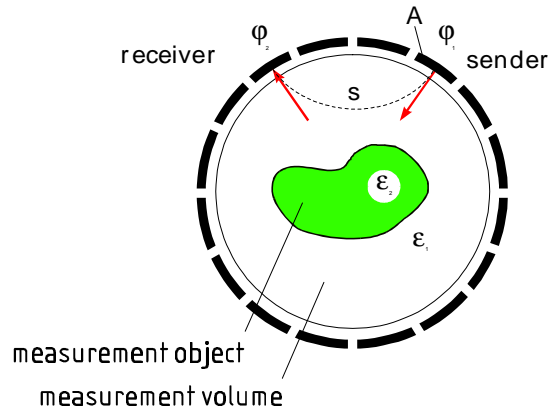


Figure 2: Measurement principle of capacitance tomography

distinguished from each other by the tomographic measurement. For instance water and air have a relation of the relative permittivity of 1:80, what makes them well distinguishable. The measurement of the capacitance can be done by different electrical measurement circuits, e.g. the sender electrode is charged and at the receiver electrode the current is measured.

The electrical field inside the measurement plane is described by the Poisson equation

$$\nabla^2 \varphi(x, y, z) + \frac{1}{\varepsilon(x, y, z)} \text{grad } \varphi(x, y, z) + \text{grad } \varepsilon(x, y, z) = \frac{\rho(x, y, z)}{\varepsilon(x, y, z)} \quad (1)$$

where $\varepsilon(x, y, z)$ denotes the permittivity and $\varphi(x, y, z)$ the electrical potential in the considered volume. The right side of equation (1) contains the source terms for free charge carrier in the measurement plane. For most applications the fluids are without electrical charge and therefore the right side of equation (1) can be set to zero. The left side of the equation consists of the equations of Laplace and Newton. The Laplace equation is valid for homogenous permittivity fields and is extended for non-homogenous permittivity fields by the Newton equation. The capacitance C is calculated by

$$C = \frac{\iint_A \varepsilon(x, y, z) \text{grad } j(x, y, z) d\hat{A}}{\int_s \text{grad } j(x, y, z) d\hat{s}} \quad (2)$$

which means the shift of the charge on the surface of an electrode divided by the difference of the potential along the way between a pair of electrodes. It is evident, from equation (1), that the relation between potential and permittivity is linear in respect to the potential, but is non-linear in respect to the permittivity. In addition the capacitance between a pair of electrodes is dependent on the permittivity field in the whole

measurement plane. This makes the reconstruction of the permittivity field much more complicated as for linear tomographic measurement systems. Linear tomographic systems are for example computer tomography, where the attenuation of an X-ray beam along a straight path is measured. Thus it is clear that the measured physical properties also have to be reconstructed also along this path.

For the non-linear capacitance tomography the measured capacitance is dependent on the permittivity field of the whole measurement plane. In addition the electrical field is distorted by the permittivity field, which results in a change of the field lines respectively the potential lines. According to equation (2), this results in a change of the capacitance. Therefore, the reconstruction for the capacitance tomography systems has to be performed with more sophisticated algorithms.

There are several reconstruction algorithms known [9]. A rather simple one is the linear backprojection algorithm which belongs to the group of the inversion techniques. For the reconstruction linearized data, the so called "sensitivity maps", are used. The sensitivity maps contain the information how much the contribution discrete element $g(x_n, y_n)$ of the property field $g(x, y)$ contributes to the measurement value for a certain combination of electrodes. The sensitivities are calculated or measured for a homogenous permittivity field inside the measurement plane which results in large reconstruction errors for non homogenous permittivity distributions. By using the sensitivity map the measurement value is distributed over the discrete elements of the reconstruction field. The advantage of this reconstruction technique is the short calculation time. However, it produces rather rough reconstruction results.

In order to improve the reconstruction, Reinecke [9] has extended the reconstruction to an iterative reconstruction technique which is depicted in Figure 3. For an assumed permittivity field the capacitances for the different electrode combinations are calculated by using a linearized field calculation. The obtained capacitances are

compared to the actual measurement values. The differences between the two is then implemented into the permittivity field by a linear optimization. For the new permittivity field the capacitances are again calculated and compared to the measurement values. This iteration is continued, until a certain error margin is reached. For the linearization and the linearized field calculation the sensitivity maps from the backprojection algorithm are used. As a result the reconstruction time is about 1 s for one image, with a reconstruction result, which is much better than for the linear backprojection. Reinecke [9] also introduced an iterative reconstruction technique by solving the Poisson equation for every permittivity distribution and using non-linear optimization. For this reconstruction technique, however, very high computation time is required.

The measurements are taken with a 16-electrode sensor for capacitance tomography. The measurement volume is axially and radially guarded by driven shield electrodes in order to obtain a homogeneous distribution of the electric field in the measurement volume and to reduce axial stray effects. The sensor is depicted in Figure 4. The axial extension of the measurement volume is 30mm. The inner diameter of the capacitance sensor is 120 mm. The measurement chain is depicted in Figure 5. The capacitances were measured using a AC-

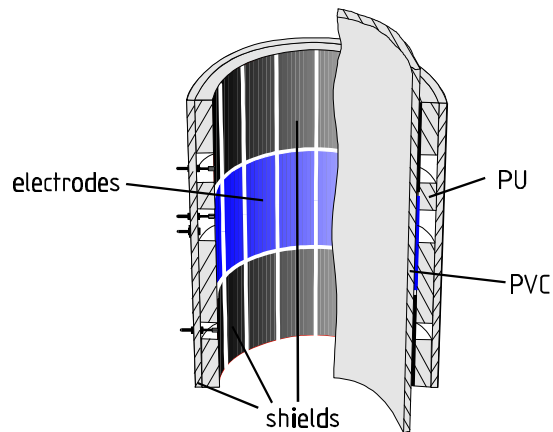


Figure 4: Schematic description of the sensor

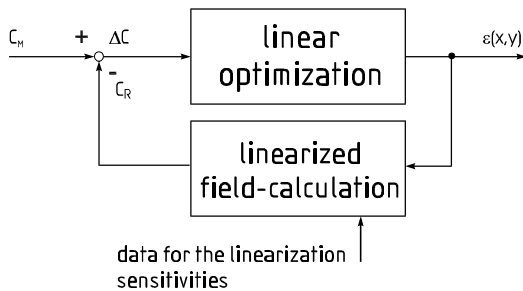


Figure 3: Principal description of the Algebraic Reconstruction Technique (ART)

balanced bridge circuit with the data-acquisition being done by A/D-converter installed on a host PC. A backprojection algorithm is installed at the PC to do a simple reconstruction for a general evaluation of the measurement values. The complete reconstruction, which needs much more computation time, is either done on a PC or on a workstation using an iterative reconstruction algorithm with a linearized electrical field calculation and a dynamic time correction of the sequential measurements [7-10].

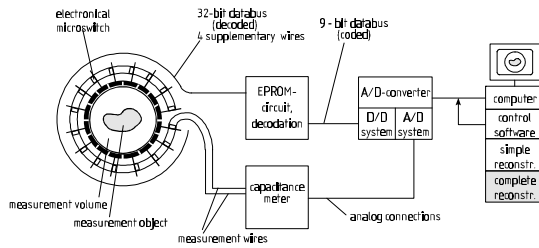


Figure 5: Measurement chain for capacitance tomography

3. EXPERIMENTAL SETUP

The measurements on structured packings with capacitance tomography are carried out in a column of 120 mm diameter. Two different types of structured packings are investigated. The structured packing Mellapak® 250.Y of Polypropylene and the gauze packing BX of Polypropylene.

For the experiments water and air is used. The water is fed into the column at the top using a liquid distributor with 36 injection nozzles to avoid maldistribution at the top of the column. The air, which is fed into the column at the bottom, is flowing upwards forced by the pressure gradient. The experimental facility is schematically depicted in Figure 6. In order to avoid distortions of the electric field from a high

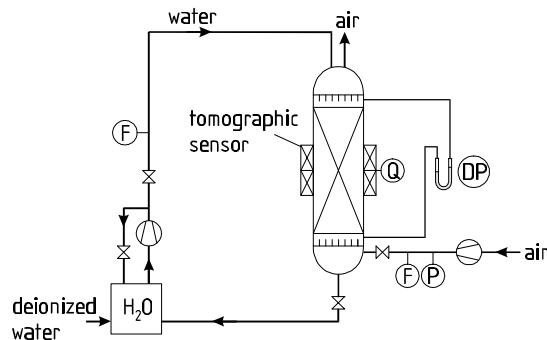


Figure 6: Experimental setup

conducting liquid phase, deionized water was used. The conductivity of water was kept below 1mS/m. Beside the tomographic measurements the pressure drop and the volumetric flow rates of the two phases are measured. The total height of the packing in the case of Mellapak® 250.Y was 1.5 m with the measuring plane of the tomographic sensor at 0.53 m above the bottom. The whole packing consists of 4 elements with 317 mm height and one element with 232 mm height. The orientation of subsequent packing elements is rotated 90°. In the case of the gauze packing BX the total height of the packing was

1.49 m and the measuring plane of the tomographic sensor was 0.53 m above the bottom. The different elements of the packing are 165 mm high and the orientation for adjacent elements is rotated 90°.

As described above, a sensor with 16 peripherally arranged electrodes was applied. For every image a total number of 72 linear independent measurements were taken sequentially at a speed of 54 images per second. The reconstruction was conducted in a field of 32x32 points with the ART algorithm described above. The maximum number of iterations for the reconstruction of each image was set to 70.

At the beginning of each measurement the capacitance of the dry packing and the capacitance of the packing full of liquid was measured. The measurements are then normalized by these boundary values. This was done for every combination of electrodes. Thus the packing itself doesn't have to be resolved by the reconstruction and the reconstructed values just describe the liquid in the packing.

4. EXPERIMENTAL RESULTS

The volume fraction of the liquid in a packing is in general denoted as the hold-up. In most publications about the applied packing types the pressure drop of the packing and in some cases the hold-up of the liquid in the packing is measured as a function of the gas and liquid load [1,2,18]. These measured values are used in the present work for the calibration of the hold-up measurements of the capacitance tomography. This is necessary because the hold-up and the measured capacitance values are non-linear. Thus the absolute values of the reconstructed hold-up are not sufficiently exact. Nevertheless the relative measurement is very useful because of the high time resolution.

4.1. Structured gauze packing BX

For the structured gauze packing the hold-up is measured as a function of time for several gas and liquid loads. In Figure 7 the liquid hold-up is depicted as a function of time for a constant liquid load and three different values of the gas load. The gas load is expressed in terms of the F-factor which is defined as

$$F\text{-factor} = w \cdot \sqrt{\rho} \quad (3)$$

where ρ denotes the density and w the superficial velocity of the gas. For small gas loads (F-factor=0.92) the hold-up is almost constant. Increasing the gas flow rate the liquid hold-up is increasing. Above the loading line the liquid hold-up is higher (F-factor=1.13) and close to the flooding point (F-factor=1.27) pulsation of the hold-up can be

observed. This pulsation, however, is very small if compared to pulsation of cocurrent two-phase flow in packings [8,9].

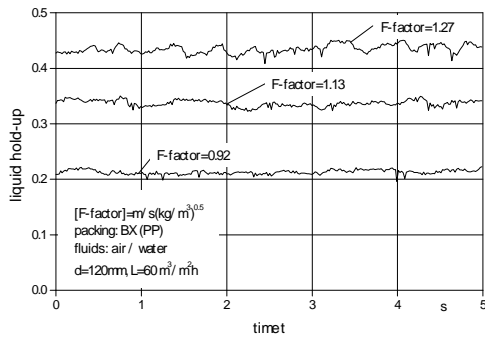


Figure 7: Liquid hold-up measured as a function of time for different gas loads

For the design of packings and distributors it is often desirable to be able to evaluate the quality of the liquid distribution on the cross section of a packed column. With the hold-up maldistribution factor

$$M_f = \frac{1}{n} \sum_{i=1}^n \left(\frac{\alpha_i - \bar{\alpha}_1}{\bar{\alpha}_1} \right)^2 \quad (4)$$

the quality of distribution can be evaluated. In Equation (4) n is the amount of sections (or pixels in the image) used for the evaluation. With α_i the local volume fraction and with $\bar{\alpha}_1$ the volume fraction of the liquid in the whole cross section is denoted. This definition of the maldistribution factor is used in literature very often in a similar form replacing the volume fraction with the local liquid mass or volume flow [16,17]. The hold-up maldistribution factor is depicted in Figure 8 as a function of time for three different gas loads. It is

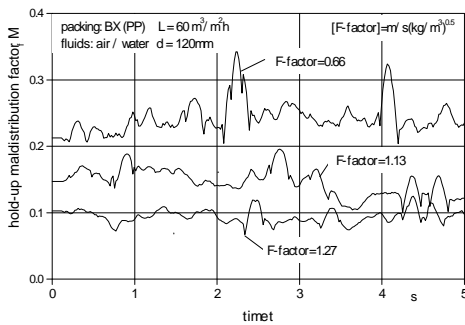


Figure 8: The maldistribution of the liquid hold-up as a function of time and gas load

obvious from the figure that the liquid maldistribution factor is decreasing if the gas load is increased. This is especially true above the loading line. Below the loading line the gas flow

has only an insignificant influence on the liquid flow.

From Figures 7 and 8 it can be concluded that for a specific gas and liquid load the liquid hold-up and the maldistribution is changing only at a small scale and that the flow can be considered as quasi-stationary. In Figure 9 the liquid distribution in the cross section of the packing is depicted for subsequent images. The time distance between two images is 18 ms. In Figure 10 the volume fraction of the liquid is depicted at the cross section of the packing for different gas loads and a constant liquid load L=60m/h. The flow regime does not change for the increasing gas flow. Only the absolute value for the liquid hold-up is increasing.

The maldistribution depicted in Figure 9 and 10 can be explained by the orientation of the sheets of the packing. The orientation of the sheets are from bottom right to top left. The liquid is flowing towards the wall and thus the liquid hold-up is increased in the areas, where the sheets end.

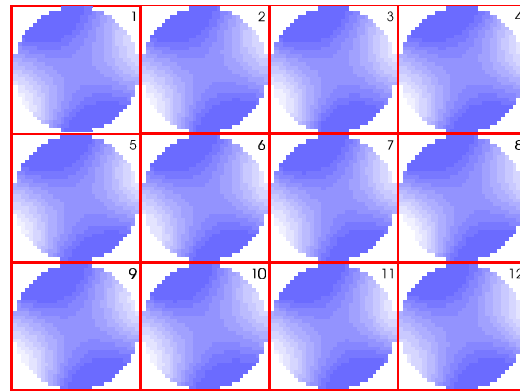


Figure 9: Local liquid hold-up for subsequent frames at a liquid load L= 60 m/h and a gas load F-factor = 1.27 m/s(kg/m³)^{0.5}

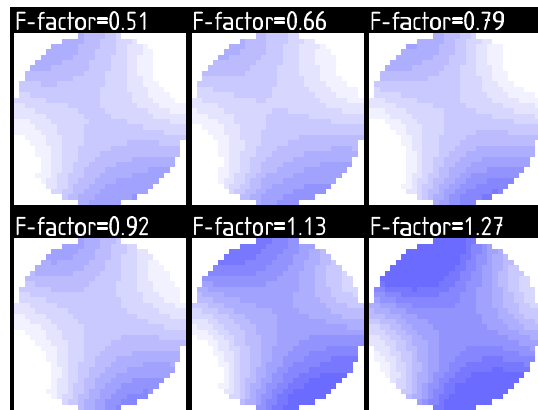


Figure 10: Local liquid hold-up for the liquid load L= 60 m/h and increasing gas loads

4.2. Structured packing Mellapak® 250.Y

For the structured packing Mellapak® 250.Y similar measurements are carried out. The liquid hold-up in the packing is measured as a function of the gas and liquid load and as a function of time. In Figure 11 the results of the hold-up

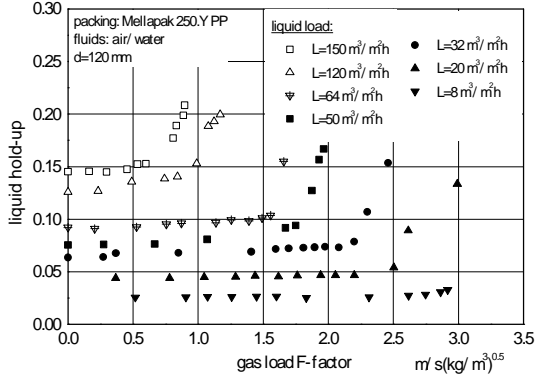


Figure 11: Liquid hold-up for different gas and liquid loads

measurements are depicted for different gas and liquid loads. The hold-up value is an integration of the local volume fraction (or local liquid hold-up) over the cross section of the column at the measurement plane. The hold-up values depicted in Figure 11 are averaged values of 500 measurements taken in 9.2 seconds. The principal measurement result is that for constant liquid load the liquid hold-up is almost constant for increasing gas load until the loading line is reached. For values of the gas load above the loading line the liquid hold-up is increasing rapidly due to the increasing momentum transfer between the phases. The hold-up increases until the flooding point is reached. For increasing liquid loads the flooding point is reached for smaller gas loads. These results are well known in literature for dumped packings [19] and for structured packings [1,2].

In Figure 12 the integral liquid hold-up is depicted as a function of time for the liquid load L=120 m/h and three different gas loads. It is shown that the liquid hold-up as well as the pulsation of the liquid hold-up is increasing for increasing gas load, especially above the loading

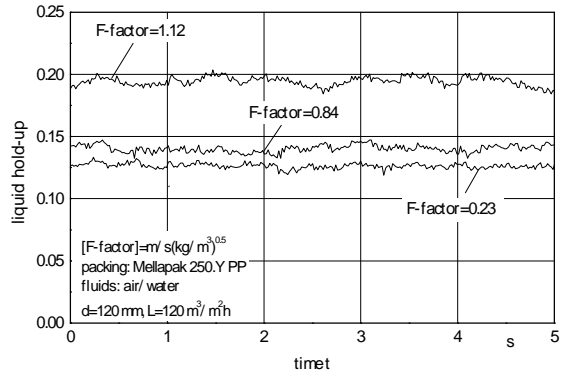


Figure 12: Liquid hold-up as a function of time for the liquid load L = 120 m/h and different gas loads

line. However, the pulsation of the liquid hold-up is small compared to the pulsation which occurs for cocurrent flow in packings [8]. Thus the hold-up in a structured packing can be considered as quasi-stationary.

As with the BX packing for the Mellapak packing the hold-up maldistribution factor M_f can be calculated from the reconstructed images according to Equation (4). The hold-up maldistribution factor is depicted in Figure 13 as a function of time for the liquid load L=50 m/h and different gas loads. The maldistribution is decreasing for increasing gas load.

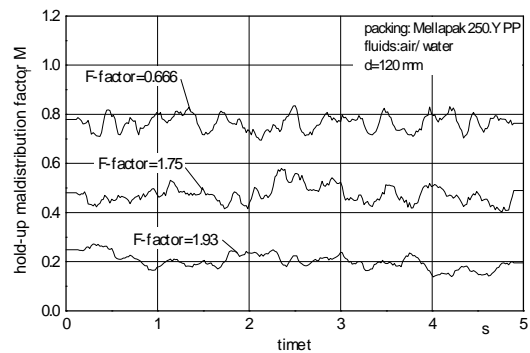


Figure 13: Hold-up maldistribution factor as a function of time for the liquid load L = 120 m/h and different gas loads

In Figure 14 the local liquid hold-up is depicted for subsequent measurements at a liquid load of $L=150$ m/h. The time step between two images is 18 ms. The local liquid load changes only at a small scale for the different time steps. It emphasizes the previously stated quasi-stationary behaviour of the flow. Also the maldistribution of the liquid phase can be seen. In analogy to the BX packing the maldistribution of the liquid is caused by the orientation of the sheets of the packing. The orientation of the sheets is from left to right at an angle of 20° . Additionally maldistribution is caused by channeling of the gas phase. At the top left side of the images in Figure 14 an area is visible, where only gas is present. This is a maldistribution of the phases which can be explained as channeling of the gas flow. In Figure 15 the local liquid hold-up is depicted for the liquid load $L = 150$ m/h and several gas loads. The distribution of the phases are similar as those depicted in Figure 14. If no gas is measured (F-factor = 0.0), only the maldistribution, which is caused by the orientation of the sheets, is observed. If the gas load is increased additional channeling can be detected. Moreover in the images in Figure 15 the increasing liquid hold-up for increasing gas loads can be observed.

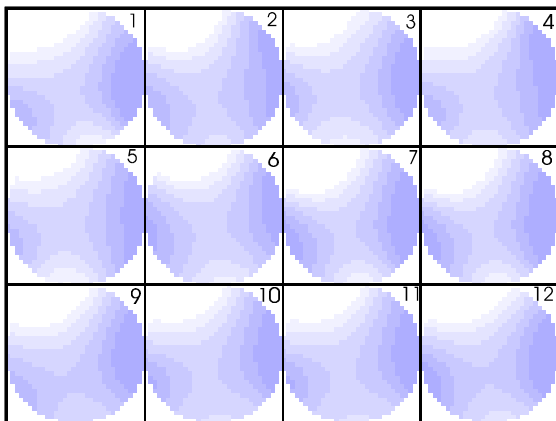


Figure 14: Local liquid hold-up at subsequent time steps for the liquid load $L = 120$ m/h and the gas load $F\text{-factor} = 1.1$ m/s(kg/m³)^{0.5}

5. CONCLUSIONS

In this work the liquid distribution in a column containing structured packings is investigated using capacitance tomography. The influence of the gas and liquid load onto the liquid hold-up and the maldistribution of the phases is discussed. The maldistribution itself can be explained from the orientation of the packing and the flow to and from the wall. For the packing Mellapak[®] 250.Y additional channeling of the gas

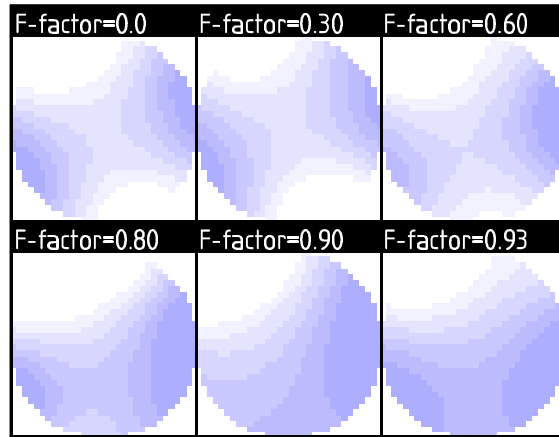


Figure 15: Local liquid hold-up for the liquid load $L = 150$ m/h and increasing gas loads

flow can be observed for high gas load. This is due to the higher cross sections of the channels compared to the channels of the BX packing. For both packings small pulsation of the hold-up can be observed close to the flooding point. However, the pulsation is very small and the flow can be considered as quasi-stationary. This means that the flow is not steady at a local scale, but at a scale of elementary cells of the packing where the values are averaged.

ACKNOWLEDGEMENTS

The authors are very grateful to Sulzer Chemtech for providing the packings and to Bayer AG for funding the research.

REFERENCES

- [1] P. Süß, L. Spiegel, "Hold-up of Mellapak structured packings", Chem. Eng. Proc., 1992, **31**, pp. 119-124
- [2] L. Spiegel, W. Meier, "Structured packings – capacity and pressure drop at very high liquid loads", Chem. Eng. Proc., 1995, **1**, pp. 36-38
- [3] N. Reinecke, G. Petristsch, D. Schmitz, D. Mewes, "Tomographic Measurement Techniques – Visualization of Multiphase Flows", Chem. Eng. Technol. 1998, **21**, 1, pp. 7-18
- [4] T. Dyakowski, S.J. Wang, C.G. Xie, R.A. Williams, M.S. Beck, "Real-Time Capacitance Imaging of Bubble Formation at the Distributor of a Fluidized Bed", in Tomographic techniques for process design and operation, Computational mechanics publications, Southampton, 1993, pp. 333-346

- [5] S.L. McKee, R.A. Williams, A. Boxman, "Development of solid-liquid mixing models using tomographic techniques", Proc. ECAPT '94, Oporto, Portugal, Process Tomography - A Strategy for Industrial Exploitation - 1994, Edts. M.S. Beck, M. S. et al, pp. 342-353.
- [6] C.G. Xie, N. Reinecke, M.S. Beck, D. Mewes, R.A. Williams, "Electrical tomography techniques for process engineering applications", Chem. Eng. J., 1994, **56** (2), pp. 127-133
- [7] N. Reinecke, D. Mewes, "Recent developments and industrial/research application of capacitance tomographie", Measurement Science and Technology, 1996, **7**, 3, pp. 233-246
- [8] N. Reinecke, D. Mewes, "Tomographic imaging of trickle-bed reactors", Chem. Eng. Sci. 1996, **51**, 10, pp. 2131-2138
- [9] N. Reinecke, "Kapazitive Tomographie für transiente Mehrphasenströmungen", Dissertation, Universität Hannover, 1996
- [10] N. Reinecke, D. Mewes, "Investigation of the two-phase flow in trickle-bed reactors using capacitance tomography", Chem. Eng. Sci. 1997, **52**, 13, pp. 2111-2127
- [11] D. Toye, P. Marchot, M. Crine, E. L'Homme, "The use of large scale computer assisted tomography for the study of hydrodynamics in trickling filters", Chem. Eng. Sci. 1994, **49**, 24b, pp. 5271-5280
- [12] N. Reinecke, D. Schmitz, D. Mewes, "X-ray tomography for two-phase flow in random and structured packings", Proc. 4th World Conference on Experimental Heat Transfer, Fluid Mechanics and Thermodynamics, ExHFT 4, 2.-6.6. 1997, Brussels
- [13] D. Schmitz, N. Reinecke, G. Petritsch, D. Mewes, "High Resolution X-ray Tomography for Stationary Multiphase Flows", Proc. OECD/CSNI Specialist Meeting on Advanced Instrumentation and Measurement Techniques, March 17.-20. 1997, Santa Barbara, CA
- [14] D. Schmitz, N. Reinecke, G. Petritsch, D. Mewes, "X-ray computed tomography for stationary multiphase flow in random and structured packings", Proc. Frontiers in Industrial Process Tomography-II, 9.-12.4.1997 Delft, The Netherlands
- [15] D. Schmitz, G. Petritsch, D. Mewes, "Tomographic Measurement of the Liquid Hold-up in a Structured Packing", Characterisation of Flow Patterns in Multiphase Flows, ASME International Congress & Exposition, 15.11.-20.11.1998, Anaheim, USA
- [16] R.M. Stikkelman, "Gas and liquid maldistribution in packed columns", Ph.D. Thesis, TU Delft, 1989
- [17] P.J. Hoek, "Large and small scale liquid maldistribution in a packed column", Ph.D. Thesis, TU Delft, 1983
- [18] E. Brunazzi, A. Paglianti, "Mechanistic Pressure Drop Model for Columns Containing Structured Packings", AIChE J. 1997, **43**, 2, pp. 317-327
- [19] R. Billet, "Packed towers in processing and environmental technology", 1995, VCH, Weinheim